Journal of Non-Crystalline Solids 618 (2023) 122545

Contents lists available at ScienceDirect

Journal of Non-Crystalline Solids

journal homepage: www.elsevier.com/locate/jnoncrysol

Insights from molecular dynamics into the chemistry-structure relationships of calcium aluminosilicate glasses

Meili Liu, Subhashree Panda, Prannoy Suraneni, Luis Ruiz Pestana *

Civil and Architectural Engineering, University of Miami, Coral Gables, FL 33146, United States

ARTICLE INFO

Keywords:
Molecular dynamics
Calcium aluminosilicate glasses
Lowenstein's rule
Topological network

ABSTRACT

Calcium aluminosilicate (CAS) glasses are ubiquitous in nature and play an important role in diverse technological applications ranging from structural glasses to sustainable cementitious materials. Understanding the relationship between the chemical composition and the structure of CAS glasses is an essential step towards optimizing their properties for different uses in the future. Here, we use extensive molecular dynamics (MD) simulations to characterize the multiscale structure of CAS glasses over the full compositional range. Analysis of the short and medium range order of the glasses reveals that Lowenstein's rule is widely violated, that silica is more susceptible than alumina to the depolymerizing effects of calcium, and that high-silica glasses favor calcium in lower oxygen coordination states, while the opposite is true for high-alumina ones. We also find the presence of highly coordinated aluminum and tricluster oxygens in high-alumina glasses, which form as a charge compensation mechanism. We find that current theoretical models used to predict oxygen species, oxygen bridge types, or tetrahedral coordination, while overall qualitatively reasonable, simplify the complex interplay between the different oxides which results in inaccurate predictions, particularly for glasses in intermediate compositional regions. Our analysis of the cluster, chain, and ring topological structures in the aluminosilicate network reveals a sharp transition from a connected to a disconnected graph which depends not only on the calcium content of the glass, but also on the ratio of silica to alumina. Glasses in the compositional region corresponding to such transition display the largest ring and longest chain structures of any glass studied.

1. Introduction

Calcium aluminosilicate (CAS) glasses, thanks to their excellent chemical, thermal, optical, and mechanical properties, find uses in diverse technological applications ranging from liquid crystal displays [1] to low-carbon alternative materials to Portland cement (the glue in concrete) [2]. As such, the structure and properties of CAS glasses have been computationally [3–8] and experimentally [9–13] studied in the past, and simple theoretical models based on stoichiometry have been proposed to predict the short- and mid-range structure of the glasses [7,14,15]. However, because most studies have focused on investigating a single or a few compositions over a narrow stoichiometric range, a holistic perspective of the chemistry-structure relationship of CAS glasses over the entire compositional space and at multiple length scales, is still lacking. For example, the compositional range over which Lowenstein's rule holds, also known as the aluminum avoidance principle (AAP), remains under debate [16–18,3,19]. Understanding the relationship between the chemical composition and the structure of CAS glasses is not only an essential step towards optimizing their properties for different uses in the future [20], but precise understanding of the molecular structure of CAS glasses is also instrumental as input to computational models to predict the glass properties, such as kinetic Monte Carlo simulations of glass dissolution [21,22].

In recent times, the topology of the aluminosilicate network has been recognized as a much more predictive descriptor of the glass properties than simple structural features or stoichiometric relationships [23,24]. Most studies aimed at characterizing the topology of glasses, however, have focused on averaged local quantities based on the statistics of oxygen bridges between network forming ions, such as the degree of depolymerization given by the NBO/T ratio [13], or the average number of topological constraints per atom [23]. Other efforts to characterize the topological medium-range order (MRO) of the glasses have focused on the ring statistics [3,25,26], which are believed to play an important, albeit unclear, role in the properties of the glass. However, the effect of glass composition on the ring size distribution is not well understood due to the difficulty of obtaining ring statistics using conventional

* Corresponding author.
E-mail address: luisruizpestana@miami.edu (L. Ruiz Pestana).

https://doi.org/10.1016/j.jnoncrysol.2023.122545
Received 1 May 2023; Received in revised form 25 June 2023; Accepted 29 July 2023
Available online 4 August 2023

experimental techniques, and the topology of the aluminosilicate network beyond local descriptors or ring statistics has not previously been investigated.

Here, we carry out extensive molecular dynamics (MD) simulations of CAS glasses over the entire ternary compositional space and characterize how the multiscale structure of the glasses depends on their chemical composition. Specifically, we quantify: (i) the short-range order (SRO), which includes the oxygen coordination of the Si/Al/Ca atoms and the populations of different oxygen species in the glass, (ii) the medium-range order (MRO), which consists of the analysis of the oxygen bridges between Al and/or Si atoms, and (iii) the topological features of the aluminosilicate network over length scales that span the whole simulated systems, thus offering a new perspective with respect to previous studies.

2. Computational methods

We carried out molecular dynamics (MD) simulations of bulk CAS glasses containing approximately 3000 atoms in a cubic simulation box. The exact number of atoms is chosen to guarantee the charge neutrality of the system, and therefore depends on the stoichiometry of the glass (Table SI-1). We simulated a total of 70 different glass compositions distributed approximately evenly over the compositional space (Fig. 1). All the results shown here are based on a single independent simulation for each glass composition. This decision was made based on our preliminary work, which showed the consistency of various structural properties across independent runs (Table SI-2). All the simulations were performed using the program LAMMPS (Large-scale Atomic/Molecular Massively Parallel Simulator package) [27]. Periodic boundary conditions (PBC) were used in all dimensions, effectively simulating bulk glasses. The interatomic interactions were described by a Born–Mayer–Huggins potential with the parameters developed by Jakse et al. [28]. This force field has been shown to reproduce structural, vibrational, and mechanical properties of CAS glasses better than those developed by Matsui [29] and Delaye [30], and in good agreement with experiments [6]. The long-range electrostatic interactions were evaluated using the particle-particle particle-mesh (PPPM) solver. Similarly to Bauchy [6], the short-range and long-range interaction cutoffs were set to 8.0 Å and 12 Å, respectively.

Following prior computational studies of CAS glasses [4–6,8,31–33], we generated bulk glasses at room temperature by simulating the process of glass solidification from a molten state as follows. First, the atoms were placed at random in the simulation box and the melt was equilibrated for 100 ps at 3000 K in the canonical ensemble (NVT), which is long enough time to lose the memory of the initial configuration. Second, the temperature was quenched down to 300 K at a cooling rate of 1 K/ps in the isothermal-isobaric ensemble (NPT) at zero pressure. Table SI-3 shows that the structural properties of the simulated glasses are not sensitive to the cooling rate from 0.1 K/ps to 10 K/ps. Additionally, the side length of the cubic simulation box was around 3 nm for all cases, and the exact dimensions of each glass are shown in Table SI-1. Finally, the equilibrated glass at the end of this cooling process was simulated for another 50 ps in the NVT ensemble at 300 K. The results shown in this paper correspond to the analysis of the 50 ps trajectories, although the relaxation dynamics of the glass at room temperature are so slow that the structural changes over the time scale of the simulation are negligible (Table SI-4).

3. Results and discussion

3.1. Short-range order (SRO)

3.1.1. Oxygen coordination of Si, Al, and Ca

We calculate the oxygen coordination number of Si, Al, and Ca atoms using cutoff values of 2.00 Å, 2.36 Å and 3 Å, respectively, which correspond to the location of the first minima in the radial distribution functions (RDFs), shown as black dash lines in Fig. SI-1. The results reported here are not sensitive to the exact values of the cutoff distances because the positions of the first peak and the first minima of the RDF are insensitive to the chemical composition of the glasses (see Table SI-5 for a quantitative analysis). As shown in Table SI-6, the coordination numbers averaged across all compositions are in good agreement with previous theoretical and experimental studies [6,34,35]. While we find Si to be always tetrahedrally coordinated, the chemical composition of the glasses plays an important role in the coordination number of both Al (Fig. 2) and Ca (Fig. 3).

Fig. 2 shows compositional ternary diagrams where the color represents the percentage of Al coordinated to four (Fig. 2B), five (Fig. 2C)

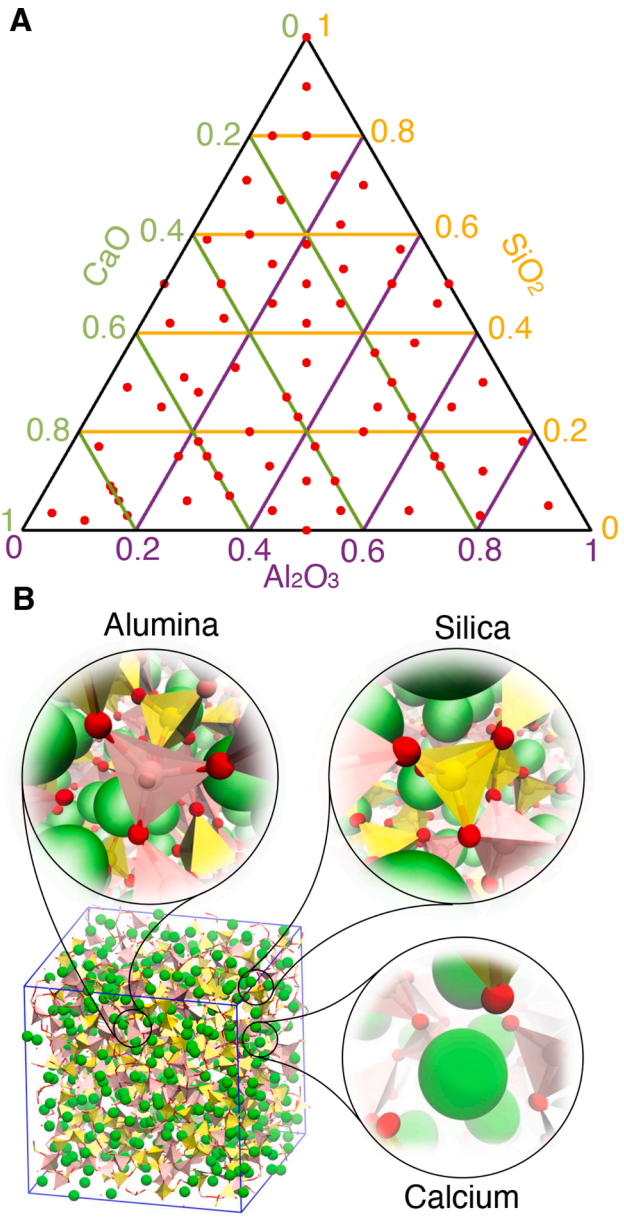

Fig. 1. (A) Compositional ternary diagram showing the glass compositions simulated in this study as red dots. The lines corresponding to constant fractions of the different oxides are shown in different colors: silica in yellow, calcium in green, and alumina in purple. The top corner corresponds to high-silica glasses, the bottom-left to high-calcium glasses, and the bottom-right to high-alumina ones. (B) A snapshot from one of the simulated glasses, illustrating the main components of CAS glasses: alumina, silica, and calcium. (For interpretation of the references to color in this figure legend, the reader is referred to the web version of this article.).

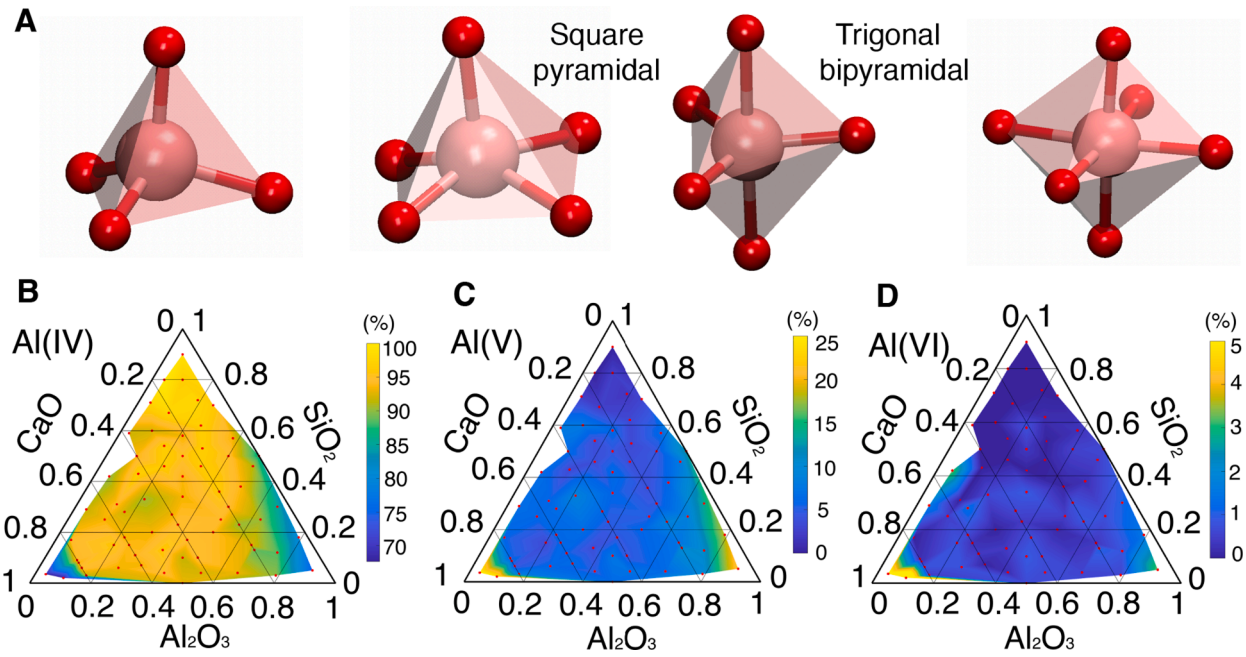

Fig. 2. Oxygen coordination of aluminum. (A) Snapshots illustrating the molecular configurations of Al(IV), Al(V), and Al(VI). (B-D) Compositional ternary diagrams showing in color the percentage of Al(IV), Al(V), and Al(VI), respectively. The range of the color scale is different for each panel.

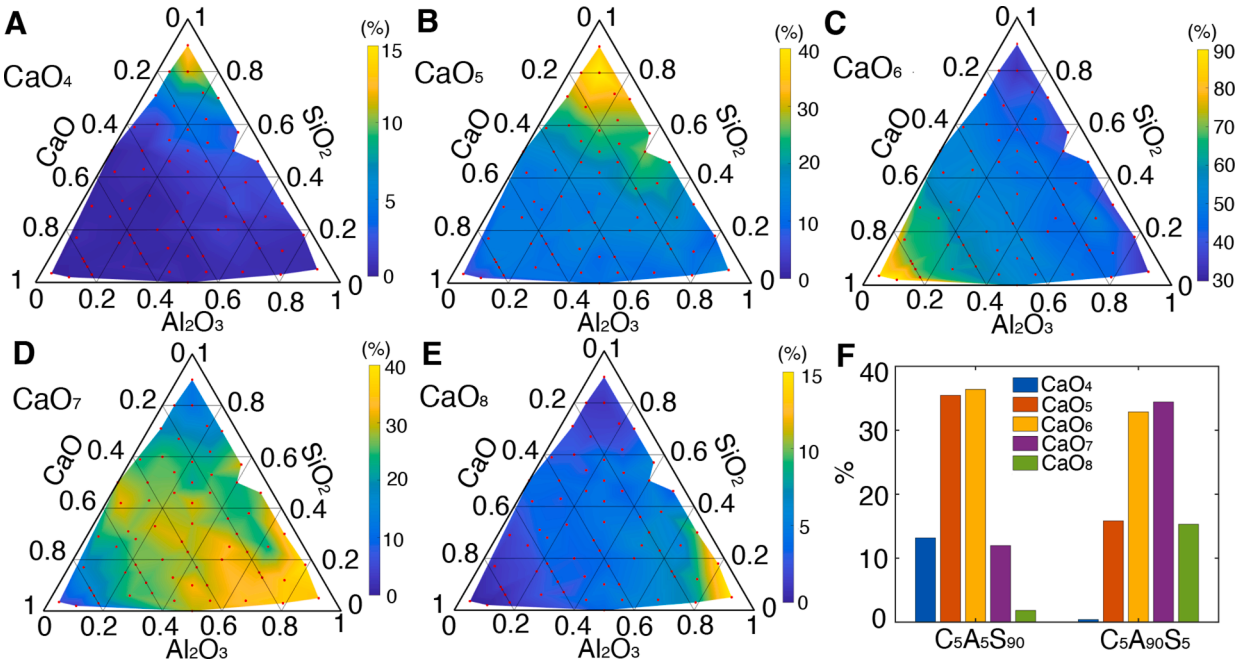

Fig. 3. Oxygen coordination of calcium ions. (A–E) Compositional ternary diagrams showing in color the percentage present in the glass of CaO_4 to CaO_8, respectively. The range of the color scale is different for each panel. (F) Percentage of calcium species in two low-calcium glasses, one high in silica and the other one high in alumina.

or six (Fig. 2D) oxygen atoms, which we refer to in what follows as Al (IV), Al(V), and Al(VI), respectively. As shown in Fig. 2A, which contains snapshots of the typical molecular structures of Al species, Al(IV) is always found tetrahedrally coordinated, Al(V) is found in either a square pyramidal or trigonal bipyramidal configuration (a structure that was suggested in a previous experimental study [13] but never confirmed), and Al(VI) is always found in an octahedral geometry. Al(IV) is, by far, the most common aluminum coordination state in CAS glasses across all compositions (Fig. 2B). Both high-calcium, and high-alumina glasses contain the highest percentages of Al(V) (20–25%), and high-calcium glasses contain the highest fraction of Al(VI) (~5%). It is worth noting that glasses in the rest of the compositional space also display non-negligible percentages of Al(V) (Fig. 3C). The presence of highly coordinated aluminum, together with the formation of tricluster oxygens (referred to as TO and discussed later in the subsection on oxygen species), have been recognized as charge compensation mechanisms alternative to the balancing effect of calcium ions on the negatively charged alumina tetrahedra [36–38].

Fig. 3 shows compositional ternary diagrams showing the populations of different calcium species, from 4 to 8-fold coordinated in

panels (A) to (E), respectively. In our simulations, we find CaO_6 to be the most common species across almost all compositions (Fig. 3A), with CaO_5 and CaO_7 being in similar proportions to CaO_6 in high-silica and high-alumina glasses, respectively. Our results are consistent with previous computational and experimental studies on both glasses and melts, which have reported a broad range of values for the average calcium coordination, from 4 to 12 (a small summary of results is shown in Table SI-6) [3–5,28,35,39]. The variability in the previously reported measurements is probably due to the fact that the local environment of Ca is much more heterogeneous than that of Si or Al due to the different nature of its interatomic interactions with oxygen. It is worth noting that none of the previous studies have been able to elucidate the effect of glass composition on the calcium coordination. We find that the percentage of CaO_6 species monotonically increases with the calcium content, and for high-calcium glasses, it is relatively insensitive to the ratio of silica to alumina in the glass (Fig. 3C). In glasses with low to moderate calcium content, however, the amount of silica in the glass relative to alumina plays a significant role on the Ca coordination (Fig. 3A–E). While high-silica glasses favor lower coordination states, CaO_5 and even CaO_4, high-alumina glasses contain highly coordinated calcium species such as CaO_7 and CaO_8. This effect is readily seen in Fig. 3F, which shows the calcium coordination of two low-calcium glasses, one high in silica and the other one high in alumina.

3.1.2. Oxygen species

Depending on the number of covalent bonds formed with network former atoms (i.e., Si and Al), which ranges from zero to three, four types of oxygen species can be identified in CAS glasses: free oxygens (FO), non-bridging oxygens (NBO), bridging oxygens (BO), and tricluster oxygens (TO). The relative populations of different oxygen species have been widely used in the past to derive metrics, such as the NBO/T ratio [1], to characterize the degree of polymerization of the aluminosilicate network. Fig. 4A–D shows the compositional ternary diagrams with the percentage of different oxygen species shown in color. Consistent with previous studies [40], only low-calcium, high-alumina glasses display significant fractions of TO, which are always bonded to Al atoms (Fig. 4A). High-silica glasses display the highest percentage of BO (Fig. 4B). As the amount of calcium in the glass increases beyond ~20%, the percentage of NBO starts to increase significantly, which is a clear sign of glass depolymerization (Fig. 4C). However, as the content of calcium increases further, beyond ~60%, the amount of NBO decreases and starts to give way to FO, the last step in the depolymerization of the glass. The percentage of FO does not seem to strongly depend on the ratio of silica to alumina in the glass (Fig. 4D). Previous work [3,17,19,41–44] has established that cations, such as Ca^{2+}, Mg^{2+}, Na^{+}, K^{+}, or Li^{+} all have a universal depolymerizing effect of the aluminosilicate network. However, whether the critical cation content at which the percentage of NBO starts to increase significantly is the same across species remains to be shown.

In Fig. 4E–H, the populations of different oxygen species obtained from the simulations are compared to the predictions of the theoretical model introduced by Yang et al. [7]. The theoretical predictions depend only on excess aluminum, $[Al_2O_3] - [CaO]$, and not on the amount of silica in the glass. Moreover, the model allows only two types of oxygen species to coexist for a given glass composition, and it assumes that both Si and Al are always tetrahedrally coordinated across the full compositional range. In contrast, our simulation results show that multiple oxygen species typically coexist in the glass, that the amount of Al(V) and Al(VI) is significant, particularly in high-calcium and/or high-alumina glasses, and that the ratio of silica to alumina impacts the structure of the glasses, particularly those with low to moderate calcium content. Therefore, although the theoretical model predicts the overall qualitative trends observed in our simulations, as a result of its limitations, it cannot capture some important characteristics of CAS glasses.

The model distinguishes between a fully depolymerized regime where $[Al_2O_3] - [CaO] < -2/3$, a fully polymerized regime for $[Al_2O_3] - [CaO] > 0$, and a partially depolymerized regime in between. In the fully depolymerized regime, the model predicts the existence of only NBO and FO, which is consistent with the simulation results. However, it overpredicts the rate at which NBO increases and FO decreases with increasing $[Al_2O_3] - [CaO]$ in this regime. In the partially depolymerized regime, the model does not account for the presence of FO,

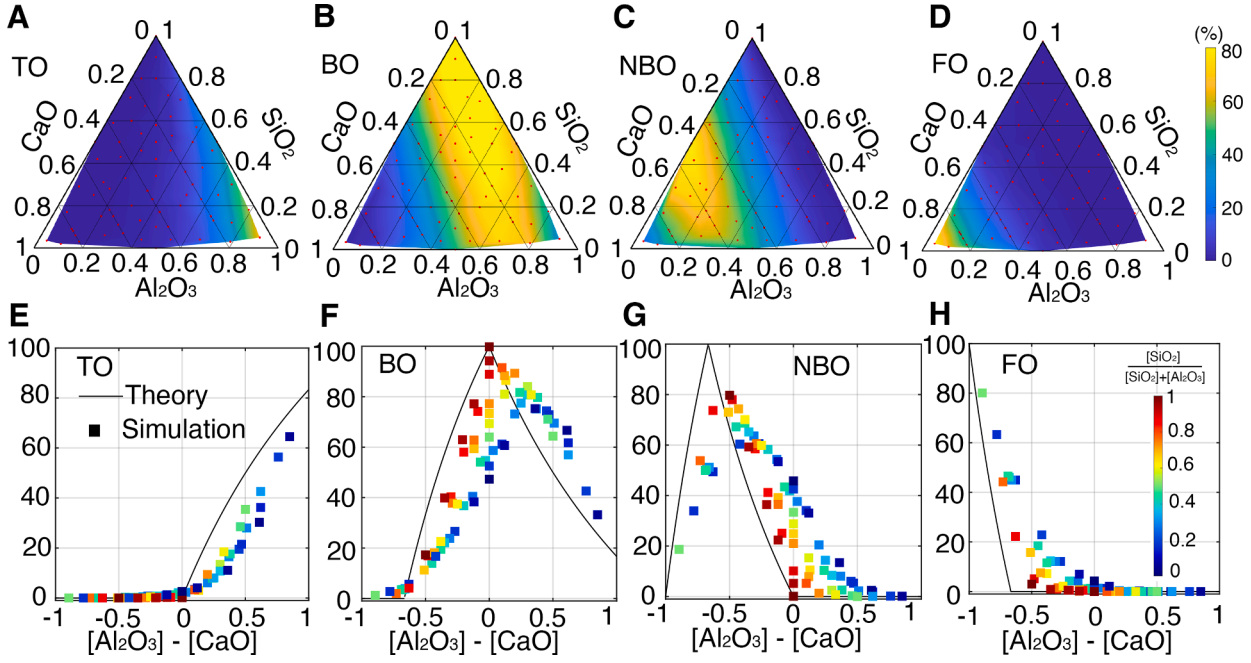

Fig. 4. Oxygen species. (A–D) Compositional ternary diagrams showing in color the percentage of the different oxygen species: tricluster oxygens (TO), bridging oxygens (BO), non-bridging oxygens (NBO), and free oxygens (FO), respectively. The range of the color scale is the same for all panels. (E–H) Comparison between the simulation results and the predictions of the theoretical model of Ref. [7]. The color of the symbols corresponding to the data from simulation indicates the relative amount of silica with respect to the total content of silica plus alumina, $[SiO_2]/([SiO_2]+[Al_2O_3])$.

which we observe in significant amounts in the simulations. As a result, in the partially depolymerized regime, the theoretical model overpredicts BO at the expense of underpredicting both FO and NBO. In other words, the glasses depolymerize faster with increasing the calcium content in the simulations than what the theoretical model predicts. In the fully polymerized regime, the model overpredicts and underpredicts the amount of TO and BO, respectively. More importantly, the model neglects the presence of NBO, which are particularly abundant in low-silica glasses (blue symbols in Fig. 4E–H). It is worth noting that the threshold $[Al_2O_3] - [CaO] = 0$, while theoretically meaningful due to the fact that the glass is supposed to be fully charge compensated when $[Al_2O_3] = [CaO]$, and thus fully polymerized, it does not reflect the reality of the simulations. For example, the theoretical model features a sharp transition for the formation of TO at $[Al_2O_3] - [CaO] = 0$, while, in the simulations, we observe that the percentage of TO grows continuously and exponentially with $[Al_2O_3] - [CaO]$ (Fig. SI-2). Decreasing the silica content of the glass at fixed $[Al_2O_3] - [CaO]$ (i.e., going from red to blue in the color scale of Fig. 4E–H) leads to a decrease in the percentage of BO and an increase in that of NBO. Interestingly, the theory seems to capture better the oxygen speciation in high-silica glasses (red symbols in Fig. 4E–H) while it fails to reproduce the simulation results for glasses with high aluminum content relative to silica (blue symbols in Fig. 4E–H).

3.2. Medium-range order (MRO)

3.2.1. Angular distribution of oxygen bridges

Fig. 5A–C presents compositional ternary diagrams displaying the average value of the angle of Si—O—Si, Si—O—Al, and Al—O—Al bridges in color, respectively. In Fig. 5, we only show compositions where the number of angles of the corresponding type is large enough to enable the calculation of the sample average with an error of ±2°. Figure SI-3A shows, for each type of bridge angle, how the standard deviation of the sample average decreases with the sample size. In Fig. SI-3B, we show the angle distribution for three glasses with very dissimilar compositions ($C_{13}A_{25}S_{62}$, $C_{12}A_{63}S_{25}$, $C_{33}A_{33}S_{33}$), which reveal well-defined but relatively broad distributions. Consistent with previous computational work [3,45] and NMR studies on silica glasses [46,47], we find $\overline{\theta}_{SiOSi} > \overline{\theta}_{SiOAl} > \overline{\theta}_{AlOAl}$ across all compositions. As the calcium content of the glass increases, $\overline{\theta}_{SiOSi}$ moderately decreases but $\overline{\theta}_{AlOAl}$ increases sharply. In regard to $\overline{\theta}_{SiOAl}$, high-alumina glasses display smaller angles than high-silica ones, although the trend is less clear. Interestingly, as shown quantitatively in Fig. 5D–F, we observe, when comparing glasses with the same amount of calcium, and where the silica content of one is equal to the alumina content of the other (e.g., $C_5A_5S_{90}$ vs $C_5A_{90}S_5$), that the number of Al—O—Al bridges is much higher than that of Si—O—Si ones (e.g., 1630 Si—O—Si bridges in $C_5A_5S_{90}$ vs. 3852 Al—O—Al bridges for $C_5A_{90}S_5$). We interpret this result as an indication that calcium preferentially disrupts Si—O—Si bridges, rather than Al—O—Al. This is further supported by the fact that the number of NBO associated with silicon atoms is always higher than that expected from just the glass stoichiometry (Fig. SI-4).

3.2.2. Oxygen bridge types

In Fig. 6, we use ternary compositional diagrams to compare the fraction of Si—O—Si, Si—O—Al, and Al—O—Al bridges measured from the simulations (Fig. 6A–C), to the prediction from a random model [3,15] (Fig. 6D–F). In the model, the fraction of bridges between m and n network former cations (Si or Al in our case) is:

$$f_{mn} = \frac{k_{m-O-n}}{\sum_{ij} k_{i-O-j}} \tag{1}$$

where $\sum_{ij} k_{i-O-j}$ is the sum over all types of bridge, which, assuming a uniform distribution of bridge types between network former cations following the stoichiometry of the glass, k_{m-O-n} can be written as:

$$k_{m-O-n} = \begin{cases} \dfrac{m \times (m-1)}{2} & m = n \\ m \times n & m \neq n \end{cases} \tag{2}$$

At a qualitative level, we observe similar trends in the simulations (Fig. 6A–C) as in the random model (Fig. 6D–F). However, the random model overpredicts the fraction of Si—O—Si and underpredicts that of Al—O—Al bridges for all compositions, with respect to the simulation

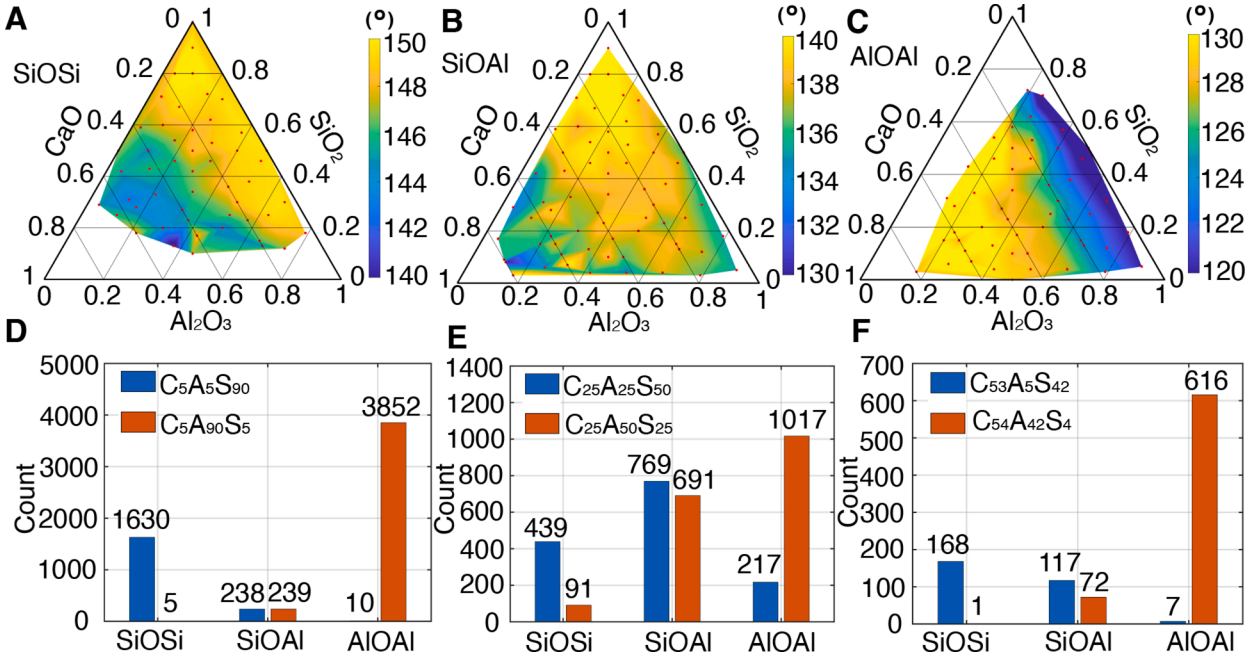

Fig. 5. Angle distribution of oxygen bridges. (A–C) Compositional ternary diagrams showing the average angles of Si—O—Si, Si—O—Al, and Al—O—Al in color, respectively. (D–F) Number of angles of each bridge type for three compositions with (D) low, (E) middle, and (F) high calcium content. Each panel compares two glasses with the same amount of calcium, and where the silica content of one is equal to the alumina content of the other.

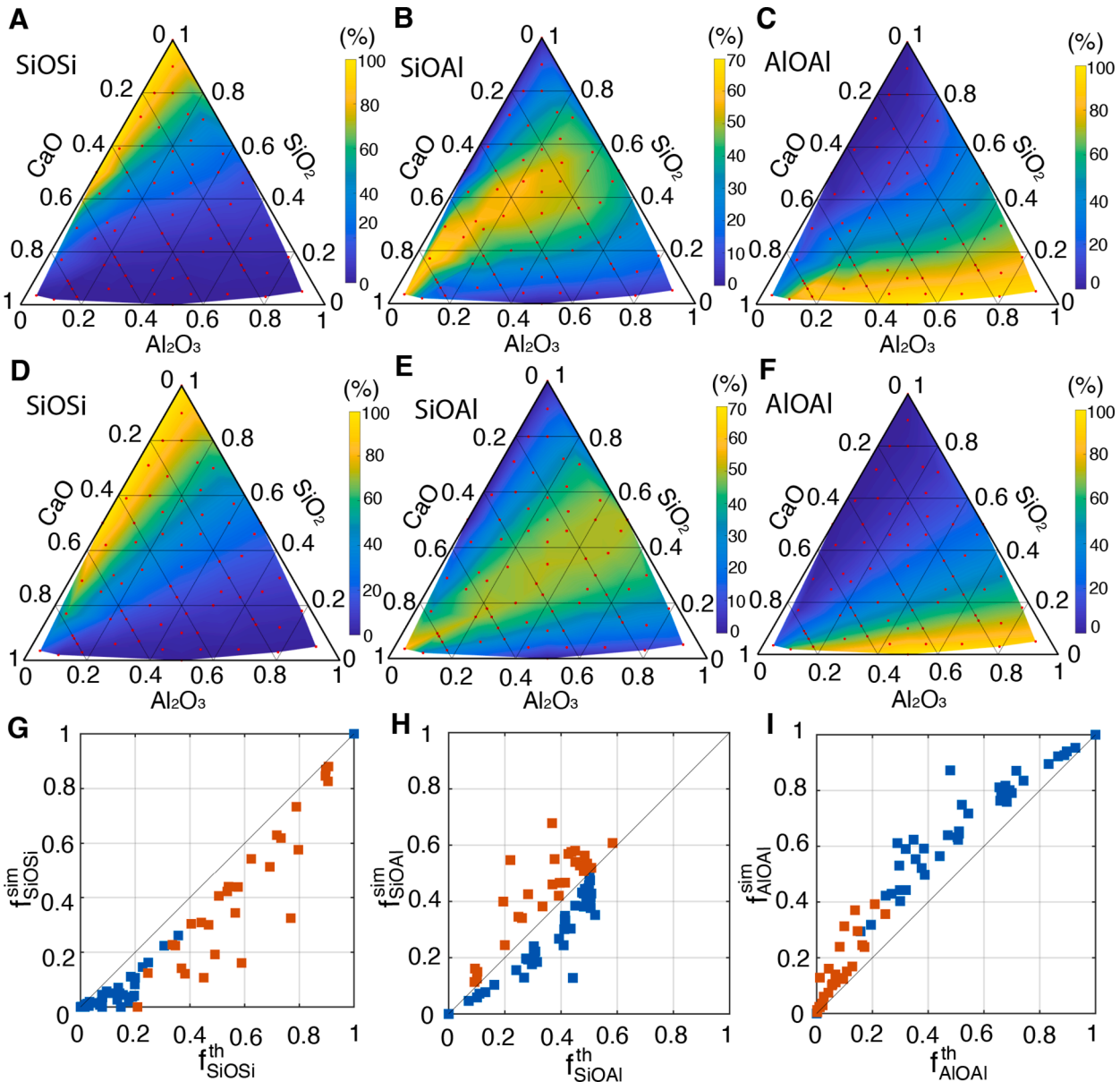

Fig. 6. Oxygen bridge types. (A–C) Compositional ternary diagrams showing in color the results from our MD simulations for the percentage of Si—O—Si, Si—O—Al, and Al—O—Al, respectively. (D–F) Predictions of the fractions of each bridge type from the random model described by Eqs. (1) and (2) [3,15]. (G–I) Direct comparison between the fraction of bridges of each type calculated in the MD simulations, f_{xOx}^{sim}, and the predictions from the random model, f_{xOx}^{RM}. The data points are shown in blue or red according to whether the random model overpredicts or underpredicts the fraction of Si—O—Al bridges observed in the simulations. (For interpretation of the references to color in this figure legend, the reader is referred to the web version of this article.).

results (Fig. 6G–I). This finding implies that the CAS glasses simulated here violate Lowenstein's rule, also known as the aluminum avoidance principle (AAP), which states that, to the point that the stoichiometry allows, the formation of Al—O—Al bridges in aluminosilicate glasses is forbidden in favor of the formation of Al—O—Si bridges. Although the issue remains contentious, widespread violations of Lowenstein's rule in aluminosilicate glasses have often been reported in the literature [6,8,17,19,42–44,48–50]. A recent experimental study [42] has even posited that current experimental results on aluminosilicate glasses necessitate breaching the Al-avoidance principle for their findings to be explained. Overall, we believe that more systematic work is necessary, particularly in the experimental domain, to validate our findings related to the widespread violation of Lowenstein's rule.

3.2.3. *Silica and alumina tetrahedral coordination*

In this section, we analyze the populations of Si(Q^n) and Al(Q^m), where n and m are the number of oxygen bridges associated with one Si or Al atom, where $n \in [0,4]$ and $m \in [0,5]$. Fig. 7 shows, as a function of [CaO], the fraction of the different Si(Q^n) (blue symbols) and Al(Q^n) (red symbols) measured from the simulations, as well as the predictions of Si (Q^n) from the theoretical statistical model first used by Eckert [14], which is sometimes also known as the binary model because it only allows the coexistence of two different Si(Q^n) in the same glass. While the theoretical predictions (black dashed line) qualitatively capture the trends of the simulation results (blue symbols) for glasses with low and moderate calcium content, the model is much less accurate for high-calcium glasses, where it assumes the glass is completely depolymerized into unconnected tetrahedra (fraction of $Q^0 = 1$). The simulations suggest a much different picture where glasses with high-calcium content still contain significant amounts of tetrahedral dimers, Si(Q^1) (Fig. 7B). In addition, while the theory predicts an almost linear decay of Si(Q^4) with calcium content, the simulations display a slightly sigmoidal

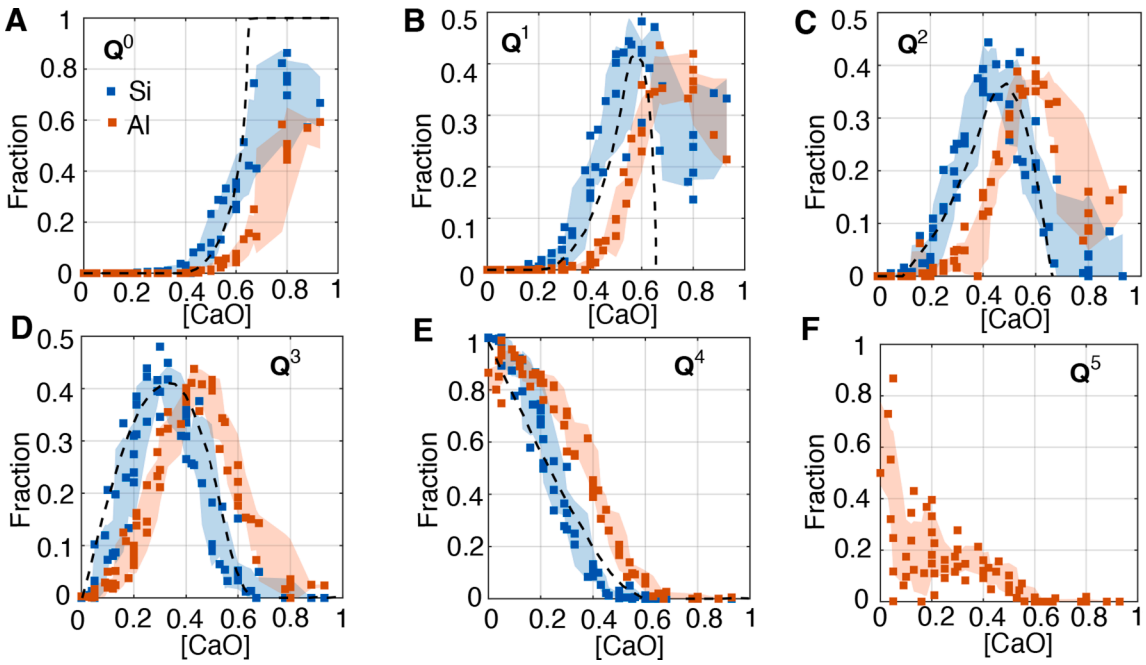

Fig. 7. Silica and alumina tetrahedral coordination. Fraction of Si (blue symbols) and Al (red symbols) associated to different numbers of bridges: (A) Q^0, (B) Q^1, (C) Q^2, (D) Q^3, (E) Q^4 and (F) Al(Q^5). The blue and red shaded areas are included as a guide for the eye and correspond to the moving average plus/minus the moving standard deviation. (For interpretation of the references to color in this figure legend, the reader is referred to the web version of this article.).

curve, where initially, for low calcium content, the decrease in the fraction of Si(Q^4) species is slow, but as calcium content in the glass increases, the decay becomes steeper, more so than what the model predicts (Fig. 7E). In Fig. SI-5, we have also compared our results to what is known as the random model [51], also finding qualitative agreement but important differences consistent with what has been noted above.

The trends that we observe for Al(Q^m), which have been widely overlooked in previous studies, are qualitatively similar to those of Si (Q^n) but with some important differences. First, the changes in Al(Q^n) with [CaO] are delayed with respect to those of Si(Q^n), suggesting that Al—O—Al bridges are less sensitive to the depolymerizing effect of Ca ions than Si—O—Si ones, which is consistent with other results shown in this work. Another important difference is that low-calcium, high-alumina glasses, which contain highly coordinated alumina, can form Al (Q^5) (inset in Fig. 7E).

3.3. Topology of the aluminosilicate network

A possible, useful representation of a CAS glass is as an undirected graph where the nodes correspond to network-forming ions, and where two nodes are connected by an edge if a bridging oxygen is shared (i.e., the edges represent oxygen bridges). In this section, we use this graph representation to systematically study the effect of chemical composition on the topology of the aluminosilicate network. Specifically, we analyze the statistics of connected clusters, chains, and rings, which are defined precisely in the following paragraphs.

We define clusters in the glass as connected graph components where two nodes belong to the same cluster if there is a path connecting them. The size of a cluster is the number of nodes in the corresponding connected graph component. Fig. 8A shows, as a function of chemical composition, the fraction of nodes that are part of the largest connected cluster in the glass, $f_{max} = N_{max}/N_{tot}$. If there is at least one path between every pair of nodes in the graph, which is known as a connected graph, there is a single cluster and $f_{max} = 1$. As the glass depolymerizes all the way into single silica or alumina units (Q^0 species), $f_{max} \to 0$. In Fig. 8A, we observe a sharp transition from a connected to a disconnected graph as the content of calcium in the glass increases. Fig. 8B shows the

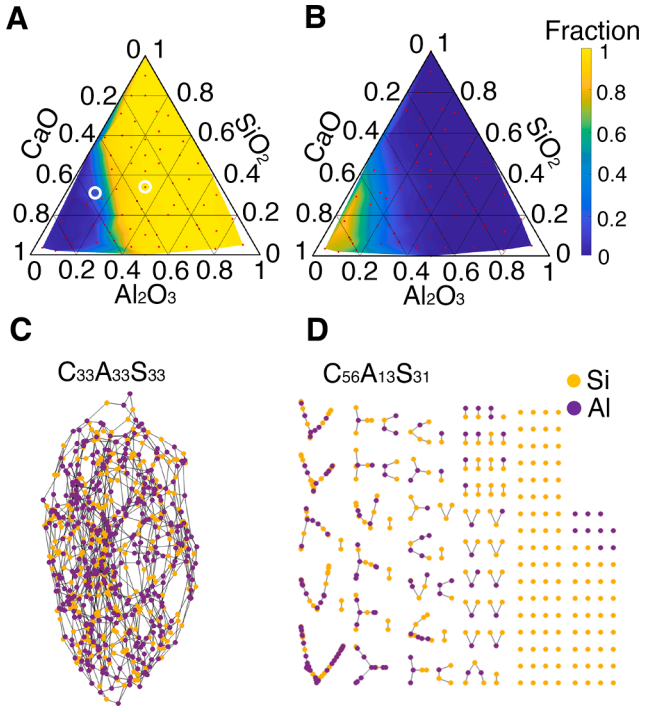

Fig. 8. Cluster analysis of the aluminosilicate network. (A) Fraction of nodes in the largest connected component (i.e., cluster) in the aluminosilicate network. (B) Fraction of nodes in clusters of size three or smaller. (C and D) Network representations of two glasses, namely $C_{33}A_{33}S_{33}$ and $C_{56}A_{13}S_{31}$, which are shown as white circles in the ternary diagram of panel (A). The alumina and silica tetrahedra are shown as yellow and purple nodes, respectively, and an edge between two nodes represents a T–O–T' bridge. The disconnected nature of the $C_{56}A_{13}S_{31}$ glass is evident. (For interpretation of the references to color in this figure legend, the reader is referred to the web version of this article.).

fraction of clusters in the system of size three or smaller, which increases rapidly as the aluminosilicate network becomes more disconnected. Interestingly, the location of this transition depends on the ratio of silica to alumina in the glass. For glasses higher in silica than alumina, the transition occurs at around 40% of calcium, while for glasses with higher alumina than silica it does so at around 60% of calcium. This is again, consistent with our previous finding that alumina is less sensitive than silica to the depolymerizing effect of calcium. The NBO/T ratio, which is broadly used as a measure of the polymerization degree of the aluminosilicate network, exhibits a similar dependence on composition albeit the transition is much smoother (Fig. SI-6). The network of two glasses, each at either side of the transition, are shown in Fig. 8C and D. It is worth noting the dramatic effect of calcium content near the transition, where a change in the calcium content of the glass of 10% or less results in systems with a completely different topological structure.

We define chains as strings of consecutive nodes with just two neighbors (i.e., one-dimensional motifs). We report as the length of the chain the number of consecutive edges, where the nodes at the ends of the chains can either have one neighbor (a free end) or more than two neighbors. In other words, chains, as defined in this work, are not necessarily isolated entities. We observe in Fig. 9, which shows the fraction of nodes in the graph that are part of chains, a pattern where the fraction of nodes in chains initially increases with calcium, reaches a maximum, and then decreases as the calcium content increases further. Interestingly, the compositional space corresponding to maximum fraction of nodes in chains coincides with the location of the transition of the aluminosilicate network from a connected to a disconnected graph. This result is consistent with the fact that, as the amount of calcium in the glass increases, the aluminosilicate network depolymerizes, which creates increasingly more open but still connected structures in the glass. As the content of calcium increases beyond the threshold at which the graph becomes disconnected ([CaO] = 40–60%), the glass network rapidly breaks down into small clusters, dimers, and monomers, which results in a sharp decrease of the fraction of nodes in chains.

We also find that, given the same calcium content, glasses higher in alumina contain a higher fraction of nodes in chains than glasses that are higher in silica, which display a denser connectivity with less chain-like structures. Our results highlight the fact that, despite both high-silica and high-alumina glasses being fully polymerized, their topological structure can be distinctly different.

We define rings as non-empty paths in the graph in which only one node (the first and last) is repeated, and where the same edge cannot be traversed twice. Furthermore, we only consider the smallest ring associated to each pair of consecutive edges. As shown in Fig. SI-7 for pure silica glass, the algorithm and criterion we use here to define rings is in good agreement with results from a previous study [52]. Overall, we observe that the number of rings decreases monotonically with increasing the calcium content of the glass (Fig. 10A). We also find that glasses with higher alumina content favor 8 and 9 membered rings, while glasses higher in silica favor 6 and 7 membered rings (Fig. 10), consistent with previous observations [3] and the fact that CAS glasses higher in alumina display more open topological structures. We also observe that high-alumina glasses favor broader distributions of ring sizes, also centered about larger ring sizes, than high-silica ones (Fig. SI-8).

Interestingly, the fraction larger rings (Fig. 10G) display a pattern that is consistent with that observed for the fraction of nodes in chains shown in Fig. 9A. This association is reasonable as larger rings will tend to contain a higher fraction of nodes in chains than smaller ones. This result is also consistent with the fact that as the amount of calcium in the glass increases, and the glass network is depolymerized, the average ring size increases. However, once the graph becomes disconnected, the fragmentation of the glass into smaller disconnected clusters breaks the rings, leading to a decrease in the average ring size. We show the average ring size as a function of calcium in Fig. 11. The rate of increase of the average ring size seems to diverge as the aluminosilicate network

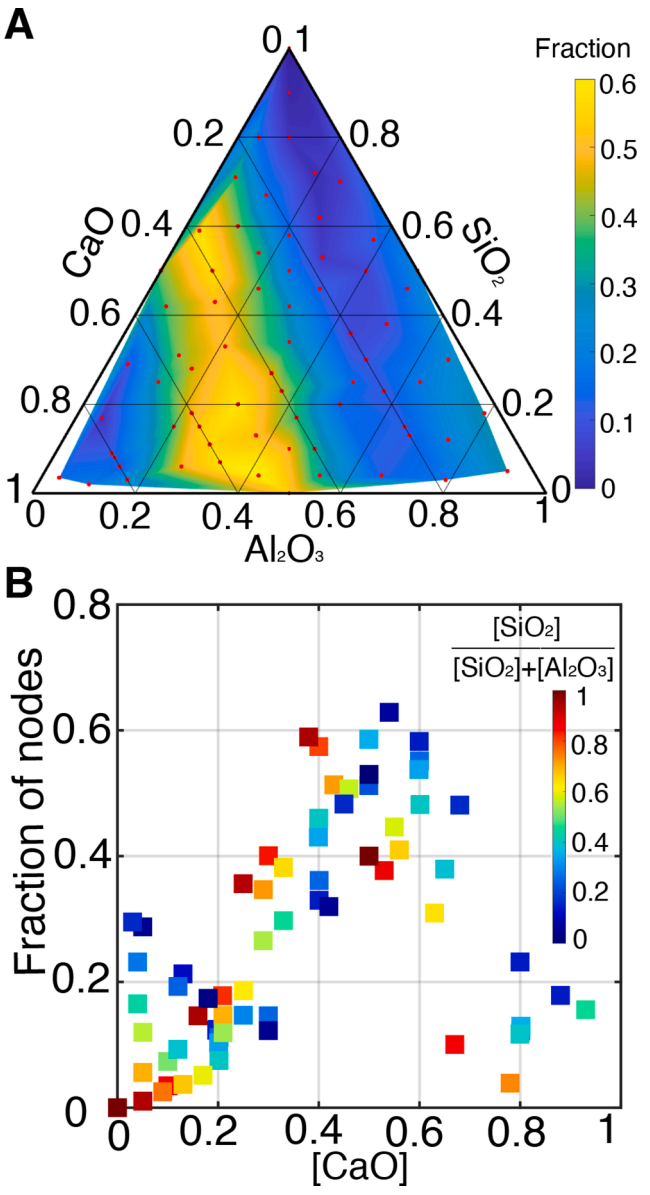

Fig. 9. Chain analysis of the aluminosilicate network. (A) Compositional ternary diagram showing in color the fraction of nodes of the graph that are part of chains. (B) Fraction of nodes in chains as a function of [CaO]. The color of the symbols corresponding to the data from simulation indicates the relative amount of silica with respect to the total content of silica plus alumina, $[SiO_2]/([SiO_2]+[Al_2O_3])$.

transitions from a connected to a disconnected graph. It is also interesting to see that while for very high-silica glasses (red in Fig. 11) the effect of increasing the content of calcium is monotonic, for very high-alumina ones (blue in Fig. 11), the average ring size initially decreases and then it increases fast. We do not find any rings in glasses with more than 80% calcium.

We expect the dramatic changes with composition of the topology of the glass to have a profound effect on its macroscopic properties, primarily due to the profoundly different nature of the inter- and intra-cluster interactions. While the dominant interatomic interactions within polymerized clusters are the covalent bonds between oxygen atoms and network-forming ions, the inter-cluster interactions are governed by electrostatics modulated by the calcium ions. For example, we expect glasses with disconnected topologies (i.e., high-calcium) to dissolve faster than those forming a connected graph (i.e., low-calcium), which has been experimentally observed [53]. Experimental

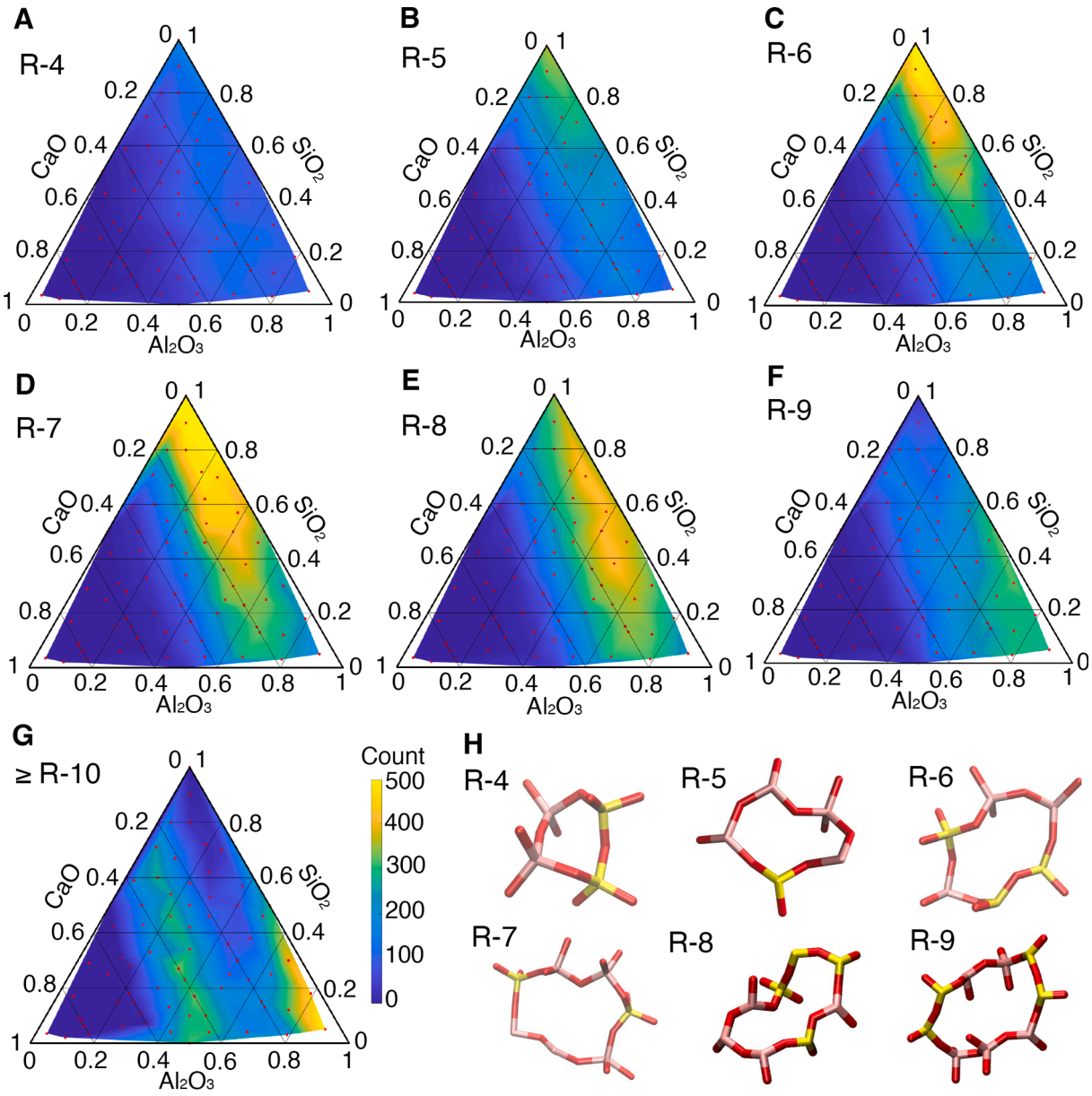

Fig. 10. Rings analysis of the aluminosilicate network. (A–G) Compositional ternary diagrams showing in color the total number of rings of each size. (H) Illustrative snapshots of rings of different sizes taken from the simulations.

measurements of the stiffness, elastic moduli and hardness of CAS glasses have revealed that glasses with high-alumina content display better mechanical properties [54], which is also consistent with our observations here. Of course, further research is needed to establish the precise relationship between the molecular structure and the emergent properties of the glass, as well as to understand the underlying mechanisms responsible for such properties.

4. Conclusions

In this work, we have performed extensive MD simulations to study the chemistry-structure relationship of calcium aluminosilicate (CAS) glasses over the full compositional range. Overall, we found the interplay between the three oxides to have a nuanced role on the structure of the glass, which is missed by current theoretical models which rely on oversimplified assumptions.

We showed that such theoretical models, although qualitatively reasonable, render inaccurate predictions particularly for glasses in intermediate compositional regions. From our short-range order (SRO) analysis, we found that the theoretical model of oxygen species significantly overpredicts the amount of bridging oxygens (BO) and underpredicts that of non-bridging oxygens (NBO) in partially depolymerized glasses. Our results showed that for glasses with low to moderate calcium content, the ratio of silica to alumina plays an important role in determining the molecular structure of the glass. For example, glasses that are higher in silica contain calcium in lower coordination states (CaO_5 and CaO_4), while in glasses higher in alumina calcium is found in higher coordination states (CaO_7 as CaO_8). We also found a significant presence of Al(V) and Al(VI), together with tricluster oxygens (TO), in high-alumina glasses, which we hypothesize, as others before us, are alternative charge compensation mechanisms when calcium is lacking in the presence of alumina.

Our medium-range order (MRO) analysis revealed that, in agreement with previous studies, the CAS glasses simulated here violated Lowenstein's rule, also known as the aluminum avoidance principle. More systematic experimental work is necessary to confirm this observation.

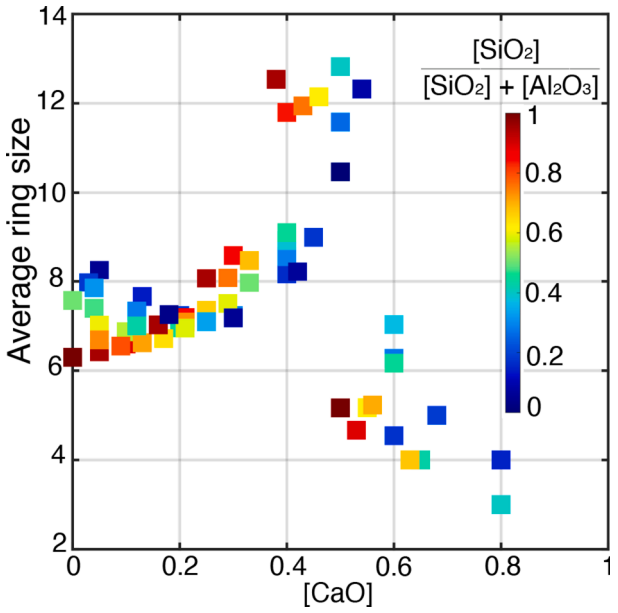

Fig. 11. Average ring size as a function of [CaO]. The color of the symbols stands for the alumina content in the glass. The color of the symbols corresponding to the data from simulation indicates the relative amount of silica with respect to the total content of silica plus alumina, $[SiO_2]/([SiO_2]+[Al_2O_3])$.

We found the fraction of Al—O—Al bridges to be higher than that predicted by a random model for all compositions. We also found that while the dependence of $Si(Q^n)$ and $Al(Q^m)$ on the calcium content of the glass follow similar trends, the changes in $Al(Q^m)$ occur at higher calcium content, which suggest that alumina is less sensitive than silica to the depolymerizing effect of calcium.

Our study of the topology of the aluminosilicate network revealed a sharp transition from a connected to a disconnected graph as the calcium content of the glass increased. Interestingly, the transition occurs at higher calcium content in glasses that are higher in alumina than those higher in silica, which is again consistent with the idea that the depolymerizing effect of calcium is less severe in alumina than silica. Our statistical analysis of chain and ring structures in the aluminosilicate network showed that as the calcium content in the glass increases, and the aluminosilicate network depolymerizes, more open structures form in the glass that are characterized by larger rings and longer chains. However, as the calcium content increases beyond the threshold of the aforementioned transition from a connected to a disconnected graph, the glass rapidly fragments into small clusters, dimers, and monomers, which in turn leads to a sharp decrease the number and size of the rings and the fraction of nodes in chains. We believe that this sharp variation of the network topology over small changes in composition, will have crucial implications on the properties of CAS glasses in ways that simple theoretical stoichiometric thresholds (e.g., $[CaO] = [Al_2O_3]$) cannot capture.

In summary, our study offers a broad and comprehensive perspective of how the chemical composition of CAS glasses determines their multiscale structure, including several aspects that have been previously overlooked. Our work constitutes an important step towards optimizing the properties of the glasses for different applications.

Supporting information

Table SI-1) Information about composition, the number of atoms, and the size of the simulation box of each simulated system. Table SI-2) Variability among independent runs of key structural properties. Table SI-3) Variability of key structural properties as a function of the cooling rate. Table SI-4) Variability in key structural properties as a function of simulation time. Table SI-5) Locations of the peaks of the RDFs measured from our simulations and the reported values from other studies. Table SI-6) Average oxygen coordination of Si, Al, and Ca measured from our simulations and the reported values from other studies. Figure SI-1) Radial distribution functions (RDFs) for Si-O, Al-O, and Ca-O. Figure SI-2) Fraction of TO as a function of excess alumina. Figure SI-3) Angular distributions of oxygen bridges for a few select glass compositions. Figure SI-4) Relationship between different oxygen species associated to Si or Al atoms. Figure SI-5) Comparison of $Si(Q^n)$ to calculated from our simulations to the theoretical predictions of the random model. Figure SI-6) Compositional ternary diagram showing in color the ratio NBO/T. Figure SI-7) Ring size distributions for pure silica. Figure SI-8) Distribution of ring sizes for a high-alumina and high-silica glass.

CRediT authorship contribution statement

Meili Liu: Formal analysis, Methodology, Software, Writing – original draft, Writing – review & editing. **Subhashree Panda:** Formal analysis, Software. **Prannoy Suraneni:** Writing – original draft, Writing – review & editing. **Luis Ruiz Pestana:** Conceptualization, Supervision, Software, Writing – original draft, Writing – review & editing.

Declaration of Competing Interest

The authors declare the following financial interests/personal relationships which may be considered as potential competing interests:

Luis Ruiz Pestana reports financial support was provided by National Science Foundation.

Data availability

Data will be made available on request.

Acknowledgments

The authors would like to thank the National Science Foundation for funding support under Grant no. 2101961. L. R. P. is also thankful for the endowment support from Dr. Reza and Georgianna Khatib and the University of Miami. P. S. gratefully acknowledges the support from the Miami Engineering Endowment at the University of Miami. All the simulations shown in this study were carried out using the supercomputer Triton, managed by the Institute of Data Science and Computing (IDSC) at the University of Miami.

Supplementary materials

Supplementary material associated with this article can be found, in the online version, at doi:10.1016/j.jnoncrysol.2023.122545.

References

[1] A. Ellison, I.A. Cornejo, Glass substrates for liquid crystal displays, Int. J. Appl. Glass Sci. 1 (1) (2010) 87–103, https://doi.org/10.1111/j.2041-1294.2010.00009.x.

[2] J. Skibsted, R. Snellings, Reactivity of supplementary cementitious materials (SCMs) in cement blends, Cem. Concr. Res. 124 (2019), 105799, https://doi.org/10.1016/j.cemconres.2019.105799.

[3] L. Cormier, D. Ghaleb, D.R. Neuville, J.-M. Delaye, G. Calas, Chemical dependence of network topology of calcium aluminosilicate glasses: a computer simulation study, J. Non-Cryst. Solids 332 (1–3) (2003) 255–270, https://doi.org/10.1016/j.jnoncrysol.2003.09.012.

[4] P. Ganster, M. Benoit, W. Kob, J.-M. Delaye, Structural properties of a calcium aluminosilicate glass from molecular-dynamics simulations: a finite size effects study, J. Chem. Phys. 120 (21) (2004) 10172–10181, https://doi.org/10.1063/1.1724815.

[5] M. Bouhadja, N. Jakse, A. Pasturel, Structural and dynamic properties of calcium aluminosilicate melts: a molecular dynamics study, J. Chem. Phys. 138 (22) (2013), 224510, https://doi.org/10.1063/1.4809523.

[6] M. Bauchy, Structural, Vibrational, and Elastic properties of a calcium aluminosilicate glass from molecular dynamics simulations: the role of the potential, J. Chem. Phys. 141 (2) (2014), 024507, https://doi.org/10.1063/1.4886421.

[7] K. Yang, Y. Hu, Z. Li, N.M.A. Krishnan, M.M. Smedskjaer, C.G. Hoover, J.C. Mauro, G. Sant, M. Bauchy, Analytical model of the network topology and rigidity of calcium aluminosilicate glasses, J. Am. Ceram. Soc. 104 (8) (2021) 3947–3962, https://doi.org/10.1111/jace.17781.

[8] G. Agnello, R. Youngman, L. Lamberson, N. Smith, W. LaCourse, A.N. Cormack, Bulk structures of silica-rich calcium aluminosilicate (CAS) glasses along the molar $CaO/Al_2O_3 = 1$ join via molecular dynamics (MD) simulation, J. Non-Cryst. Solids 519 (2019), 119450, https://doi.org/10.1016/j.jnoncrysol.2019.05.026.

[9] A. Steimacher, N.G.C. Astrath, A. Novatski, F. Pedrochi, A.C. Bento, M.L. Baesso, A. N. Medina, Characterization of thermo-optical and mechanical properties of calcium aluminosilicate glasses, J. Non-Cryst. Solids 352 (32) (2006) 3613–3617, https://doi.org/10.1016/j.jnoncrysol.2006.03.091.

[10] M. Moesgaard, R. Keding, J. Skibsted, Y. Yue, Evidence of intermediate-range order heterogeneity in calcium aluminosilicate glasses, Chem. Mater. 22 (15) (2010) 4471–4483, https://doi.org/10.1021/cm1011795.

[11] R. Snellings, Surface chemistry of calcium aluminosilicate glasses, J. Am. Ceram. Soc. 98 (1) (2015) 303–314, https://doi.org/10.1111/jace.13263.

[12] L. Hennet, J.W.E. Drewitt, D.R. Neuville, V. Cristiglio, J. Kozaily, S. Brassamin, D. Zanghi, H.E. Fischer, Neutron diffraction of calcium aluminosilicate glasses and melts, J. Non-Cryst. Solids 451 (2016) 89–93, https://doi.org/10.1016/j.jnoncrysol.2016.05.018.

[13] R. Zhang, Z. Wang, Y. Meng, S. Jiao, J. Jia, Y. Min, C. Liu, Quantitative insight into aluminum structures in $CaO–Al_2O_3–SiO_2$ system via Raman and ^{27}Al MAS-NMR spectroscopies, J. Non-Cryst. Solids 573 (2021), 121116, https://doi.org/10.1016/j.jnoncrysol.2021.121116.

[14] H. Eckert, Structural characterization of noncrystalline solids and glasses using solid state NMR, Prog. Nucl. Mag. Res. Spectrosc. 24 (3) (1992) 159–293, https://doi.org/10.1016/0079-6565(92)80001-V.

[15] Y. Zhao, J. Du, X. Cao, C. Zhang, G. Xu, X. Qiao, Y. Liu, S. Peng, G. Han, A modified random network model for $P_2O_5–Na_2O–Al_2O_3–SiO_2$ glass studied by molecular dynamics simulations, RSC Adv. 11 (12) (2021) 7025–7036, https://doi.org/10.1039/D0RA10810C.

[16] E.R. Myers, V. Heine, M.T. Dove, Thermodynamics of Al/Al avoidance in the ordering of Al/Si tetrahedral framework structures, Phys. Chem. Miner. 25 (6) (1998) 457–464, https://doi.org/10.1007/s002690050136.

[17] S.K. Lee, J.F. Stebbins, The degree of aluminum avoidance in aluminosilicate glasses, Am. Mineral. 84 (5–6) (1999) 937–945, https://doi.org/10.2138/am-1999-5-630.

[18] S.K. Lee, J.F. Stebbins, Al–O–Al and Si–O–Si sites in framework aluminosilicate glasses with $Si/Al = 1$: quantification of framework disorder, J. Non-Cryst. Solids 270 (1) (2000) 260–264, https://doi.org/10.1016/S0022-3093(00)00089-2.

[19] S.K. Lee, H.-I. Kim, E.J. Kim, K.Y. Mun, S. Ryu, Extent of disorder in magnesium aluminosilicate glasses: insights from ^{27}Al and ^{17}O NMR, J. Phys. Chem. C 120 (1) (2016) 737–749, https://doi.org/10.1021/acs.jpcc.5b10799.

[20] P.H. Gaskell, Structure and properties of glasses—How far do we need to go? J. Non-Cryst. Solids 222 (1997) 1–12, https://doi.org/10.1016/S0022-3093(97)90091-0.

[21] L Ruiz Pestana, S Shantha Raju, C Guntoorkar, P Suraneni, Kinetic Monte Carlo Study on the Role of Heterogeneity in the Dissolution Kinetics of Glasses, J. Phys. Chem. C 127 (16) (2023) 7695–7701, https://doi.org/10.1021/acs.jpcc.3c01123.

[22] Sebastien Kerisit, Du Jincheng, Monte Carlo simulation of borosilicate glass dissolution using molecular dynamics-generated glass structures, J. Non-Cryst. 522 (2019), 119601.

[23] M. Bauchy, Deciphering the atomic genome of glasses by topological constraint theory and molecular dynamics: a review, Comput. Mater. Sci. 159 (2019) 95–102, https://doi.org/10.1016/j.commatsci.2018.12.004.

[24] H. Liu, T. Zhang, N.M. Anoop Krishnan, M.M. Smedskjaer, J.V. Ryan, S. Gin, M. Bauchy, Predicting the dissolution kinetics of silicate glasses by topology-informed machine learning, NPJ. Mater. Degrad. 3 (1) (2019) 1–12, https://doi.org/10.1038/s41529-019-0094-1.

[25] S. Le Roux, P. Jund, Ring statistics analysis of topological networks: new approach and application to amorphous GeS_2 and SiO_2 systems, Comput. Mater. Sci. 49 (1) (2010) 70–83, https://doi.org/10.1016/j.commatsci.2010.04.023.

[26] Y. Shi, J. Neuefeind, D. Ma, K. Page, L.A. Lamberson, N.J. Smith, A. Tandia, A. P. Song, Ring size distribution in silicate glasses revealed by neutron scattering first sharp diffraction peak analysis, J. Non-Cryst. Solids 516 (2019) 71–81, https://doi.org/10.1016/j.jnoncrysol.2019.03.037.

[27] in 't A.P. Thompson, H.M. Aktulga, R. Berger, D.S. Bolintineanu, W.M. Brown, P. S. Crozier, P.J. Veld, A. Kohlmeyer, S.G. Moore, T.D. Nguyen, R. Shan, M. J. Stevens, J. Tranchida, C. Trott, S.J. Plimpton, LAMMPS—A flexible simulation tool for particle-based materials modeling at the atomic, meso, and continuum scales, Comput. Phys. Commun. 271 (2022), 108171, https://doi.org/10.1016/j.cpc.2021.108171.

[28] N. Jakse, M. Bouhadja, J. Kozaily, J.W.E. Drewitt, L. Hennet, D.R. Neuville, H. E. Fischer, V. Cristiglio, A. Pasturel, Interplay between non-bridging oxygen, triclusters, and fivefold Al coordination in low silica content calcium aluminosilicate melts, Appl. Phys. Lett. 101 (20) (2012), 201903, https://doi.org/10.1063/1.4766920.

[29] M. Matsui, Molecular dynamics study of the structures and bulk moduli of crystals in the system $CaO-MgO-Al_2O_3-SiO_2$, Phys. Chem. Miner. 23 (6) (1996) 345–353, https://doi.org/10.1007/BF00199500.

[30] J.-M. Delaye, L. Cormier, D. Ghaleb, G. Calas, Investigation of multicomponent silicate glasses by coupling WAXS and molecular dynamics, J. Non-Cryst. Solids 293–295 (2001) 290–296, https://doi.org/10.1016/S0022-3093(01)00680-9.

[31] F. Mauri, A. Pasquarello, B.G. Pfrommer, Y.-G. Yoon, S.G. Louie, Si–O–Si bond-angle distribution in vitreous silica from first-principles ^{29}Si NMR analysis, Phys. Rev. B 62 (8) (2000) R4786–R4789, https://doi.org/10.1103/PhysRevB.62.R4786.

[32] M. Bouhadja, N. Jakse, A. Pasturel, Striking role of non-bridging oxygen on glass transition temperature of calcium aluminosilicate glass-formers, J. Chem. Phys. 140 (23) (2014), 234507, https://doi.org/10.1063/1.4882283.

[33] J. Du, A.N. Cormack, The medium range structure of sodium silicate glasses: a molecular dynamics simulation, J. Non-Cryst. Solids 349 (2004) 66–79, https://doi.org/10.1016/j.jnoncrysol.2004.08.264.

[34] V. Petkov, Th. Gerber, B. Himmel, Atomic ordering in $Ca_{x/2}Al_xSi_{1-x}O_2$ glasses ($x = 0,0.34,0.5,0.68$) by energy-dispersive X-ray diffraction, Phys. Rev. B 58 (18) (1998) 11982–11989, https://doi.org/10.1103/PhysRevB.58.11982.

[35] V. Petkov, S.J.L. Billinge, S.D. Shastri, B. Himmel, Polyhedral units and network connectivity in calcium aluminosilicate glasses from high-energy X-ray diffraction, Phys. Rev. Lett. 85 (16) (2000) 3436–3439, https://doi.org/10.1103/PhysRevLett.85.3436.

[36] R.S. Welch, S. Astle, R.E. Youngman, J.C. Mauro, High-coordinated alumina and oxygen triclusters in modified aluminosilicate glasses, Int. J. Appl. Glass Sci. 13 (3) (2022) 388–401, https://doi.org/10.1111/ijag.16565.

[37] D.R. Neuville, L. Cormier, A.-M. Flank, V. Briois, D. Massiot, Al speciation and Ca environment in calcium aluminosilicate glasses and crystals by Al and Ca K-edge X-ray absorption spectroscopy, Chem. Geol. 213 (1–3) (2004) 153–163, https://doi.org/10.1016/j.chemgeo.2004.08.039.

[38] D.R. Neuville, L. Cormier, D. Massiot, Al coordination and speciation in calcium aluminosilicate glasses: effects of composition determined by ^{27}Al MQ-MAS NMR and Raman spectroscopy, Chem. Geol. 229 (1–3) (2006) 173–185, https://doi.org/10.1016/j.chemgeo.2006.01.019.

[39] R.S. Welch, K.-H. Lee, C.J. Wilkinson, M. Ono, C.B. Bragatto, J.C. Mauro, Topological hardening through oxygen triclusters in calcium aluminosilicate glasses, J. Am. Ceram. Soc. 104 (12) (2021) 6183–6193, https://doi.org/10.1111/jace.18032.

[40] S.R. Astle, R.S. Welch, C.J. Wilkinson, M.L. Bødker, K.A. Kirchner, M. M. Smedskjaer, J.C. Mauro, Modeling oxygen tricluster formation in calcium aluminosilicate supercooled liquids and glasses, J. Phys. Chem. B 126 (40) (2022) 8039–8047, https://doi.org/10.1021/acs.jpcb.2c03949.

[41] H. Jabraoui, Y. Vaills, A. Hasnaoui, M. Badawi, S. Ouaskit, Effect of sodium oxide modifier on structural and elastic properties of silicate glass, J. Phys. Chem. B 120 (51) (2016) 13193–13205, https://doi.org/10.1021/acs.jpcb.6b09664.

[42] A.R. Allu, A. Gaddam, S. Ganisetti, S. Balaji, R. Siegel, G.C. Mather, M. Fabian, M. J. Pascual, N. Ditaranto, W. Milius, J. Senker, D.A. Agarkov, V.V. Kharton, J.M. F Ferreira, Structure and crystallization of alkaline-earth aluminosilicate glasses: prevention of the alumina-avoidance principle, J. Phys. Chem. B 122 (17) (2018) 4737–4747, https://doi.org/10.1021/acs.jpcb.8b01811.

[43] S.K. Sharma, B. Simons, H.S. Yoder Jr, Raman study of anorthite, calcium tschermak's pyroxene, and gehlenite in crystalline and glassy states, Am. Mineral. 68 (11–12) (1983) 1113–1125.

[44] J.B. Murdoch, J.F. Stebbins, I.S.E. Carmichael, High-resolution ^{29}Si NMR study of silicate and aluminosilicate glasses: the effect of network-modifying cations, Am. Mineral. 70 (3–4) (1985) 332–343.

[45] B. Mihailova, N. Zotov, M. Marinov, J. Nikolov, L. Konstantinov, Vibrational spectra of rings in silicate glasses, J. Non-Cryst. Solids 168 (3) (1994) 265–274, https://doi.org/10.1016/0022-3093(94)90338-7.

[46] R.F. Pettifer, R. Dupree, I. Farnan, U. Sternberg, NMR determinations of Si–O–Si bond angle distributions in silica, J. Non-Cryst. Solids 106 (1–3) (1988) 408–412, https://doi.org/10.1016/0022-3093(88)90299-2.

[47] I. Farnan, P.J. Grandinetti, J.H. Baltisberger, J.F. Stebbins, U. Werner, M. A. Eastman, A. Pines, Quantification of the disorder in network-modified silicate glasses, Nature 358 (6381) (1992) 31–35, https://doi.org/10.1038/358031a0.

[48] A. Atila, E.M. Ghardi, A. Hasnaoui, S. Ouaskit, Alumina effect on the structure and properties of calcium aluminosilicate in the percalcic region: a molecular dynamics investigation, J. Non-Cryst. Solids 525 (2019), 119470, https://doi.org/10.1016/j.jnoncrysol.2019.119470.

[49] S. Ganisetti, A. Gaddam, R. Kumar, S. Balaji, G.C. Mather, M.J. Pascual, M. Fabian, R. Siegel, J. Senker, V.V. Kharton, J. Guénolé, N.M.A. Krishnan, J.M.F. Ferreira, A. R. Allu, Elucidating the formation of Al–NBO bonds, Al–O–Al linkages and clusters in alkaline-earth aluminosilicate glasses based on molecular dynamics simulations, Phys. Chem. Chem. Phys. 21 (43) (2019) 23966–23977, https://doi.org/10.1039/C9CP04332B.

[50] M. Benoit, S. Ispas, M.E. Tuckerman, Structural properties of molten silicates from ab initio molecular-dynamics simulations: comparison between $CaO-Al_2O_3-SiO_2$ and SiO_2, Phys. Rev. B 64 (22) (2001), 224205, https://doi.org/10.1103/PhysRevB.64.224205.

[51] G.N. Greaves, S. Sen, Inorganic glasses, glass-forming liquids and amorphizing solids, Adv. Phys. 56 (1) (2007) 1–166, https://doi.org/10.1080/00018730601147426.

[52] Q. Zhou, Y. Shi, B. Deng, J. Neuefeind, M. Bauchy, Experimental method to quantify the ring size distribution in silicate glasses and simulation validation

thereof, Sci. Adv. 7 (28) (2021), eabh1761, https://doi.org/10.1126/sciadv.abh1761.

[53] A. Schöler, F. Winnefeld, M.B. Haha, B. Lothenbach, The effect of glass composition on the reactivity of synthetic glasses, J. Am. Ceram. Soc. 100 (6) (2017) 2553–2567, https://doi.org/10.1111/jace.14759.

[54] A. Pönitzsch, M. Nofz, L. Wondraczek, J. Deubener, Bulk elastic properties, hardness and fatigue of calcium aluminosilicate glasses in the intermediate-silica range, J. Non-Cryst. Solids 434 (2016) 1–12, https://doi.org/10.1016/j.jnoncrysol.2015.12.002.